Mathematical Modelling of Weld Phenomena 6, Institute of Materials, London, UK. 2002.

Scaling Laws in the Welding Arc

P. F. Mendez, M. A. Ramirez, G. Trapaga, T. W. Eagar
Department of Materials Science and Engineering
Massachusetts Institute of Technology
Cambridge, MA 02139

ABSTRACT

The technique of order of magnitude scaling (OMS) [1] has been applied to the mathematical modeling of a long electric arc. The estimations obtained are combined with numerical calculations, thus important features of both techniques are considered simultaneously: the high precision of numerical modeling, and the generality and simplicity of algebraic expressions. Power-law expressions for the estimations of length of the transition region, maximum radial and axial velocity, maximum pressure in the cathode spot, maximum temperature in the column and arc radius are obtained and are consistent with previous theoretical and experimental work. The calculations of arc temperature differ from channel models of the arc by considering the heat transfer in the gas region surrounding the arc.

I. INTRODUCTION

The main goal of this work is to demonstrate the application of the new technique of Order of Magnitude Scaling (OMS) [1, 2] to the welding arc. OMS is a framework for the approximate solution wide variety of complex problems with many driving forces described by a set of differential equations. It provides closed form estimations of the unknowns in a problem, their range of validity, and a set of dimensionless groups that indicate the true ratio of driving forces. These results are obtained even when the problems are described by non-linear partial differential equations. OMS focuses on problems with many driving forces, it does not present convergence problems, and can be much faster than methods that numerically integrate the governing equations.

OMS is related to scaling and approximation work in the fields of mathematics [3-6], engineering [7-10], and artificial intelligence [11-25]. OMS differs from work in mathematics in that it solves only for the characteristic values of the unknown functions instead of solving for all values over the domain. From engineering approaches, OMS borrows the use of dimensionless groups and the emphasis on characteristic values, and it differs in the use of matrix algebra and the rules for normalization of functions. OMS is similar to approaches in Artificial Intelligence in that it can be implemented in the form of a computer algorithm. OMS and Artificial Intelligence also share some common concepts, such as a description of the dominant physics of the problem in a space of parameters. OMS differs from Artificial Intelligence in that it can deal with partial differential equations and that it uses matrix algebra instead of sets of rules or constraints.

OMS has two main stages, the first one is representing the governing equations in matrix form: the matrix of coefficients. The second stage involves iterations and matrix operations that solve for the unknowns, provide the range of validity of the approximations, and determine the quality of the approximations. Obtaining the matrix of coefficients is the task that requires the most judgment from the engineer. After a system has been captured in the matrix of coefficients, an iterative method must be used to determine what driving forces are dominant. This iterative

method assumes that some driving forces are dominant, and tests these hypotheses for self-consistency with matrix operations involving the matrix of coefficients.

Previous attempts have been made to provide general and simple expressions that capture the behavior of the arc. In this work we will include a review of OMS of the fluid flow in the transition region of the arc [26]. Other general expressions have been derived using dimensional analysis or asymptotic analysis [27-35] and from analysis of results obtained from mathematical models[36, 34, 37-40]. The results obtained herein are consistent with the existing literature; however, this work reaches further by presenting new closed form expressions for the arc radius and column temperature.

II. DESCRIPTION OF THE PROBLEM

This paper focuses on the fluid flow in the transition region and on the temperature field in the column region. The transition region, represented in Fig. 1, is defined as that contained within R_C in the radial direction and extending for a length of Z_S beyond the cathode boundary layer in the axial direction. A long arc is such that the position of the anode has little effect on the behavior of the transition region. A convenient way to define the characteristic length Z_S is:

$$Z_S = V_{ZS} / \max\left(\partial V_Z / \partial Z\right) \tag{1}$$

The cathode spot radius can be calculated as $R_C = \left(I/\pi J_C\right)^{1/2}$, where the critical current density J_C depends mainly on the electrode temperature for thermo-ionic electrodes (for the numerical simulations it was assumed J_C = 6.5 10^7 A/m^2 [41] for a tungsten electrode, and J_C = 4.4 10^7 A/m^2 [42] for a graphite electrode).

The governing equations used are the equation of conservation of mass (2), conservation of momentum in the R and Z components respectively (3 and 4), conservation of energy (E1), Ampère's law in R and Z respectively (5 and 6), and conservation of magnetic field (8).

$$\frac{1}{R}\frac{\partial}{\partial R}(RV_R)+\frac{\partial V_Z}{\partial Z}=0 \tag{2}$$

$$\rho\left(V_R\frac{\partial V_R}{\partial R}+V_Z\frac{\partial V_R}{\partial Z}\right)=-\frac{\partial P}{\partial R}+\mu\left[\frac{\partial}{\partial R}\left(\frac{1}{R}\frac{\partial}{\partial R}(RV_R)\right)+\frac{\partial^2 V_R}{\partial Z^2}\right]-J_Z B \tag{3}$$

$$\rho\left(V_R\frac{\partial V_Z}{\partial R}+V_Z\frac{\partial V_Z}{\partial Z}\right)=-\frac{\partial P}{\partial Z}+\mu\left[\frac{1}{R}\frac{\partial}{\partial R}\left(R\frac{\partial V_Z}{\partial R}\right)+\frac{\partial^2 V_Z}{\partial Z^2}\right]+J_R B \tag{4}$$

$$\begin{aligned}\rho C_p\left(V_R\frac{\partial T}{\partial R}+V_Z\frac{\partial T}{\partial Z}\right)&=k\left[\frac{1}{R}\frac{\partial}{\partial R}\left(R\frac{\partial T}{\partial R}\right)+\frac{\partial^2 T}{\partial Z^2}\right]+\\&+\frac{J_R{}^2}{\sigma}+\frac{J_Z{}^2}{\sigma}-S_R+\frac{5}{2}\frac{k_b}{e}\left(J_R\frac{\partial T}{\partial R}+J_Z\frac{\partial T}{\partial Z}\right)\end{aligned} \tag{5}$$

$$\mu_0 J_R=-\frac{\partial B}{\partial Z} \tag{6}$$

$$\mu_0 J_Z=\frac{1}{R}\frac{\partial}{\partial R}(RB) \tag{7}$$

$$\frac{\partial^2 B}{\partial Z^2}+\frac{\partial}{\partial R}\left[\frac{1}{R}\frac{\partial}{\partial R}(RB)\right]=0 \tag{8}$$

In these equations the assumptions are: isothermal plasma (therefore constant density and viscosity values corresponding to the maximum temperature in the transition region), axisymmetric, laminar flow, steady state (this implies a DC arc, or slow current variations), and no magnetic convection because the magnetic Reynolds number is very small. The magnetic Reynolds number is a measure of the ratio between the induced magnetic field (due to the conductive fluid motion) and the imposed magnetic field [43]; its expression in this problem is $\mathrm{Re_m} = V_{ZS} Z_S \sigma_e \mu_0$, and varies between 10^{-3} and 10^{-1} for the cases studied here. The boundary conditions for the scaling of the system are listed in Tables I, II, and III.

III. SCALING OF THE ELECTROMAGNETIC FIELD

Because constant properties are used for calculating the fluid flow, the governing equations for the electromagnetic field can be decoupled. The equations for the electromagnetic field contain the set of parameters μ_0, R_c, J_c, R_i, and h, and only two dimensionless groups are

necessary to describe this system: h/R_C, and R_i/R_C. The boundary conditions for the scaling of the electromagnetic field are represented in Table I. Previous knowledge about the problem, from experiments and numerical models, indicates that the functions vary smoothly within the corner points outlining the transition region; this is an important requirement for the application of OMS.

The functions describing the electromagnetic field can be scaled with the following relationships:

$$R = R_i r' \tag{9}$$

$$Z = hz' \tag{10}$$

$$J_R(R,Z) = J_{RS} j_r(r',z') \tag{11}$$

$$J_Z(R,Z) = J_C j_z(r',z') \tag{12}$$

$$B(R,Z) = \tfrac{1}{2}\mu_0 \frac{{R_C}^2}{R_i} J_C r' \left[1 + \left(\frac{{R_i}^2}{{R_C}^2} - 1 \right) b(r',z') \right] \tag{13}$$

where

$$B_S = \tfrac{1}{2}\mu_0 \frac{{R_C}^2}{R_i} J_C$$

The scaling factors R_i, h, J_{RS}, J_C, and B_S are characteristic values, of which R_i and J_{RS} are unknown. The scaling of $B(R, Z)$ is such that $b(r',z') = 1$ at point **B** in Fig. 1, $b(r',z') = 0$ at point **J** in Fig. 1, and $B(R, Z)$ increases linearly at R=0, as eq. (6) to (8) indicate. The radius of the anode spot (R_i) depends on the electrical properties of the plasma, which are determined by heat transfer in the arc. The characteristic value J_{RS} could be estimated by balancing equation (6). Normally for welding arcs, $\Delta R / R_C > 1$, where $\Delta R = R_a - R_C$. The scaling relationships above are valid for flat or almost flat tip electrodes. The dominant component of the radial current density in sharper electrodes is given directly by the critical current density generated by thermionic emission.

When these scaling relationships are replaced into the governing equations for the electromagnetic field (equations (6) to (8)), the estimation of the characteristic radial current density J_{RS} can be obtained from equation (6) using the dominant balance technique.

$$\hat{J}_{RS} = \begin{cases} J_C \dfrac{R_c \Delta R}{h R_i} & \text{for } \dfrac{\Delta R}{R_C} < 1 \\ J_C \dfrac{\Delta R^2}{h R_i} & \text{for } \dfrac{\Delta R}{R_C} \geq 1 \end{cases} \tag{14}$$

IV. SCALING OF FLUID FLOW

The equations governing the coupled electromagnetic field and fluid flow in the transition region (eq. (2) to (8)) contain the following set of parameters ρ, μ, μ_0, R_c, J_c, R_i, h, and R_e. The set of dimensionless groups related to the fluid flow is Re, h/R_C, R_i/R_C, and R_e/R_C, where $\mathrm{Re} = \rho \hat{V}_{ZS} \hat{Z}_S / \mu$. Because R_i is the only element of parameter that depends on heat transfer in the arc, the dimensionless group R_i/R_C will be neglected in this isothermal formulation of the fluid flow. The group R_e/R_C is also of little importance, because its influence is confined mainly to the cathode boundary layer, outside the transition region. The boundary conditions for the scaling of the fluid flow are represented in Table II. Current knowledge about the problem, from experiments and numerical models, indicates that the functions vary smoothly within the corner points.

The functions describing fluid flow can be scaled with the following relationships:

$$R = R_C r \tag{15}$$

$$Z = \delta + Z_S z \tag{16}$$

$$V_R(R,Z) = V_{RS} r v_r(r,z) \tag{17}$$

$$V_Z(R,Z) = V_{ZS}\left[v_{z0}(z) - f_{VZ2}(\mathrm{Re}, h/R_C) r^2 v_z(r,z)\right] \tag{18}$$

$$P(R,Z) = P_S p(r,z) \tag{19}$$

The scaling of $V_Z(R, Z)$ is such that it varies in a quadratic manner in R at R=0, as eq. (2) to (4) indicate. These scaling relationships are replaced into the governing equations for the fluid flow (equations (2) to (4)), for the application of the dominant balance technique. This technique determines that the inertial forces are balanced by the plasma pressure and the electromagnetic forces in the equation of conservation of momentum in the radial direction, and that the plasma pressure balances the inertial forces in the equation of conservation of momentum in the axial direction. Viscous effects are secondary. With the dominant and balancing forces established, the characteristic values Z_S, V_{RS}, V_{ZS}, and P_S can be estimated as:

$$\hat{Z}_S = \tfrac{1}{2} R_C \tag{20}$$

$$\hat{V}_{RS} = \tfrac{1}{2} \frac{\mu_0^{1/2} R_C J_C}{\rho^{1/2}} \tag{21}$$

$$\hat{V}_{ZS} = \tfrac{1}{2} \frac{\mu_0^{1/2} R_C J_C}{\rho^{1/2}} \tag{22}$$

$$\hat{P}_S = \tfrac{1}{2} \mu_0 R_C^{\,2} J_C^{\,2} \tag{23}$$

The estimations above are valid when all of the terms in the normalized governing equations (eq. (2) to (8)) have a magnitude of one or less. This is true for $\mathrm{Re} > 1$, $R_i/R_C > 2$, and $h/R_C > \tfrac{1}{2}\Delta R^2/(R_i R_C)$. In order to further simplify the problem and avoid the effects of the anode on the transition region, an additional condition is necessary: $h/Z_S >> 1$. These conditions are met for all of the cases considered in the present analysis.

V. SCALING OF THE TEMPERATURE FIELD

For the scaling of the temperature field it will be assumed that convection is not important in the column, in a similar fashion of channel arc models. This is reasonable, considering that the temperature profile in the column of a long arc is fairly uniform, as indicated in Figure 2, and the Prandtl number of the arc is smaller than one, indicating that heat is transmitted faster than momentum. The same hypothesis is made in the Elenbaas-Heller equation[34]. Neglecting convection allows us to decouple the temperature field from the fluid flow. The parameters that govern the temperature field are then k_T, σ_T, S_{RT}, (5/2 k_b/e), ($I\Delta R/\pi h$), ($2I/\pi$), k_g, S_{Rg}, and T_i, and the corresponding natural dimensionless groups are

$$\frac{\text{conduction}}{\text{radiation}} = k_T^{\,0.2}\sigma_T^{\,0.3}S_{RT}^{\,-0.7}\left(\frac{2}{\pi}I\right)^{-0.6}k_g^{\,0.4}S_{Rg}^{\,0.4}\left(T_i - T_0\right)^{0.4}$$

$$\frac{\text{Joule radial}}{\text{radiation}} = \left(\frac{I\Delta R}{\pi h}\right)^2\left(\frac{2}{\pi}I\right)^{-2}$$

$$\frac{\text{electron drift}}{\text{radiation}} = k_T^{\,-0.6}\sigma_T^{\,0.6}S_{RT}^{\,-0.4}\left(\frac{5}{2}\frac{k_b}{e}\right)\left(\frac{I\Delta R}{\pi h}\right)\left(\frac{2}{\pi}I\right)^{-1.2}k_g^{\,0.3}S_{Rg}^{\,0.3}\left(T_i - T_0\right)^{0.3}$$

The model presented here differs from standard channel arc models in that the domain is split in two concentric cylindrical domains as indicated in Figure 3. The core contains the plasma and is limited by a characteristic "ionization" temperature. This core is surrounded by another gaseous cylinder, with a wall thickness determined by the temperature gradient outside the core.

The scaling relationships for the inner cylinder are:

$$R = R_i r' \tag{24}$$

$$T(R) = T_i + T_C\theta'(r') \tag{25}$$

and for the outer cylinder

$$R = \Delta R_g r''$$ (26)

$$T(R) = T_0 + (T_i - T_0)\theta''(r'')$$ (27)

Since the arc is transparent to radiation, and convection is negligible, the only way energy is transmitted to the outer cylinder is by conduction, expressed by the following relationship:

$$k_T \frac{T_C^{\,2}}{R_i} = k_g \frac{T_i - T_0}{\Delta R_g}$$ (E1)

which considers that the properties of the plasma are dependent on the temperature. This dependence will be characterized by a ionization temperature and a slope, defined in Fig. 4.

Thus:

$$S_R = S_{RT}(T - T_i)$$ (28)

$$k = k_T(T - T_i)$$ (29)

$$\sigma = \sigma_T(T - T_i)$$ (30)

In the gas of the outer core, the gas has no electrical conductivity and the thermal properties will be approximated as constant, thus:

$$S_R = S_{Rg}$$ (31)

$$k = k_g$$ (32)

Applying the scaling relationships to the equation of energy in each region, and performing successive dominant-balance operations to find a self-consistent combination, we obtain that in the core cylinder the energy input is dominated by axial component of Joule heating, and the energy output is dominated by radiation. In the outer cylinder, the energy input is by conduction and the energy output is again by radiation in the gas. These concepts lead to the following estimations:

$$\hat{R}_i = {k_T}^{0.2} {\sigma_T}^{-0.2} {S_{RT}}^{-0.2} \left(\frac{2}{\pi} I\right)^{0.4} {k_g}^{-0.1} {S_{Rg}}^{-0.1} \left(T_i - T_0\right)^{-0.1} \tag{33}$$

$$\hat{T}_C = {k_T}^{-0.4} {\sigma_T}^{-0.1} {S_{RT}}^{-0.1} \left(\frac{2}{\pi} I\right)^{0.2} {k_g}^{0.2} {S_{Rg}}^{0.2} \left(T_i - T_0\right)^{0.2} \tag{34}$$

$$\Delta\hat{R}_g = {k_g}^{0.5} {S_{Rg}}^{-0.5} \left(T_i - T_0\right)^{0.5} \tag{35}$$

VI. NUMERICAL ANALISIS

The formulation of the numerical model is also represented by the conservation equations (2)-(8) described above, plus an equation for the conservation of energy with the assumption of local thermodynamic equilibrium (LTE). Since the numerical model covers the whole domain and is not confined to only represent the transition region, the boundary conditions include the cathode, the anode, and the column regions. The equation of conservation of energy includes the temperature dependence of thermophysical properties. The additional boundary conditions required to represent the system are summarized in Table IV, and include the following assumptions:

- Non slip conditions at the surface of the electrodes (zero velocity values)
- The temperatures at the electrodes are assumed constant at 2500 K on the anode and 4000 K on the cathode [44].
- The boundary conditions must reflect the symmetry condition of no flow across the axis (line AD in Fig. 1).
- The magnetic flux density, B, at the cathode is obtained assuming a constant value of Jc in the cathode spot of known radius, but is zero outside this spot.

In a typical calculation, a grid of 60 x 60 nodes was employed and each calculation normally took about 2 hours of CPU time on a Pentium II-333 processor.

Table V summarizes the characteristic values for the fluid flow obtained numerically for a number of arc cases ranging from 200 A to 2160 A and including properties of argon and air plasmas.

VII. DISCUSSION

Fig. 5 shows a comparison of the estimations for fluid flow in the transition region using equations (20) to (23) with characteristic values obtained from the numerical analysis described above. Fig. 6 shows a comparison of the estimations for temperature field in the column region using equations (33) to (35) with characteristic values obtained from the numerical analysis described above and several other numerical and experimental sources[36, 45, 41, 46-49, 38]. The properties of the plasma are contained in Table V and Table VI.

This comparison spans a range of currents of more than one order of magnitude. A regression that relates the measured or calculated values versus the estimations provides an indication of the quality of the estimation. Table VII indicates the coefficient and R^2 for these regressions. The coefficient indicates the ratio measured/estimated or calculated/estimated; in all cases this coefficient is of the order of magnitude of 1, indicating that the estimations predict the correct order of magnitude. The best prediction of the order of magnitude is for V_{ZS}, while the difference is larger for Z_S, V_{RS}, and P_S. One possible reason for this discrepancy is that the magnitudes associated with the fluid flow are sensitive to the aspect ratio of the transition region. This aspect ratio was estimated to within a factor of 3.6, and this error propagates error into the other magnitudes. The error in the estimation of Z_S is likely to be related to the assumption that the cathode boundary layer is very thin. This simplification can introduce a measurable error, especially for lower currents.

The correlation (R^2) indicates how much of the variations in the measured or calculated behavior is explained by the scaling factor. In all but two cases the scaling factor explains more than 90% of the behavior of the system.

The small fraction of the trends not captured by the scaling factor are due to two sources. One is numerical or experimental error, and the other is that all secondary driving forces have been neglected in the estimations. These secondary forces are divided into two classes, whether they were included in the governing equations or not. Those driving forces considered in the governing equations are characterized by "natural dimensionless groups," which consist of the ratio of a given driving force to the dominant force. The other secondary forces can be quantified with dimensionless groups constructed *ad hoc*, based on intuition.

The natural dimensionless groups associated with the governing equations used in this work are usually smaller than 10%, indicating that their contribution is small. This is consistent with the good correlations obtained and suggests that no important driving forces have been neglected. The scatter is larger for the scaling of the temperature in the column ($\hat{T}_C$), and the length of the gradient in the gas ($\Delta\hat{R}_g$).

The estimation for temperature in the column ($\hat{T}_C$) explains only 37% of the variations, and the estimation for the length of the gradient in the gas ($\Delta\hat{R}_g$) has a correlation close to zero. For these two cases we have estimated the correct order of magnitude but captured of the trends poorly. There are two possible causes for this; one is that important driving forces have been left out of the governing equations, the other is numerical or experimental error. These two magnitudes show the smallest variations for the cases analyzed, and this can magnify numerical and experimental error out of proportion. This is a likely source of the scatter, especially considering the good agreement for the arc radius, which is obtained simultaneously with these other two estimations. More refined estimations of the temperature field, including convection should prove or disprove this hypothesis.

The estimations obtained for maximum velocity and pressure have the same functional form as those previously proposed [28, 33, 34]. These estimations were extracted from the original set of governing equations by using the OMS technique, without the need to solve the original system of differential equations, neither to impose functional forms of the solutions nor to assume a priori which the dominant forces are.

VIII. CONCLUSIONS

The focus of this paper involved the application of order of magnitude scaling technique (OMS) to represent the behavior of an electric arc. The analysis of the fluid flow is centered in the transition region, where momentum and electromagnetic phenomena are dominant and temperature effects can be appropriately disregarded. The analysis of the temperature field focuses on the plasma column outside the transition region, where convective heat transfer is much smaller than radiation losses. The results obtained using OMS are compared with

numerical models and experiments covering two different gases and a wide range of currents and arc lengths.

The main conclusions of this work can be summarized as follows:

- In the transition region the viscous effects are small, and the radial and axial inertial forces balance the electromagnetic pressure created by the flow of the current through the plasma.
- The radius of the arc is calculated by considering the heat transfer effect of the gas region surrounding the plasma.
- In the arc column the plasma main energy input is Joule heating in the *Z*-direction, and the main energy loss is through radiation.
- In the gas region the main energy input is conduction from the arc and the main energy loss is radiation.
- The estimations of the characteristic values of maximum velocity and maximum pressure obtained through OMS have the same expression as previous analytical expressions determined by Maecker [28] and Allum [33], with the exception of a factor of $\sqrt{2}$ for the expression of axial velocity. This factor makes Equation (22) more accurate than Maecker's equivalent.
- The estimations of the maximum velocity and pressure in the transition region are given by the following equations:

$$\hat{V}_{RS} = \tfrac{1}{2}\frac{\mu_0^{1/2} R_C J_C}{\rho^{1/2}}$$

$$\hat{V}_{ZS} = \tfrac{1}{2}\frac{\mu_0^{1/2} R_C J_C}{\rho^{1/2}}$$

$$\hat{P}_S = \tfrac{1}{2}\mu_0 R_C^{\,2} J_C^{\,2}$$

- The estimations of the radius and maximum temperature in the column are given by the following equations:

$$\hat{R}_i = {k_T}^{0.2} {\sigma_T}^{-0.2} {S_{RT}}^{-0.2} \left(\frac{2}{\pi} I\right)^{0.4} {k_g}^{-0.1} {S_{Rg}}^{-0.1} \left(T_i - T_0\right)^{-0.1}$$

$$\hat{T}_C = {k_T}^{-0.4} {\sigma_T}^{-0.1} {S_{RT}}^{-0.1} \left(\frac{2}{\pi} I\right)^{0.2} {k_g}^{0.2} {S_{Rg}}^{0.2} \left(T_i - T_0\right)^{0.2}$$

NOTATION

A summary of the magnitudes, associated functions, characteristic values, and estimations used in the formulation of the problem is presented in Table VIII. The other symbols used in this work are:

e: charge of the electron

h: arc length

I: welding current

J_c: current density at cathode

k_b: Boltzman's constant

k_g: thermal conductivity of gas at the ionization temperature

k_T: temperature coefficient of the thermal conductivity of the plasma

R_c: cathode spot radius

R_e: radius of electrode

Re: Reynolds number

$\mathrm{Re_m}$: magnetic Reynolds number

R_i: arc radius (measured at ionization temperature)

S_{Rg}: radiation losses of the gas at the ionization temperature

S_{RT}: temperature coefficient of the radiation losses of the plasma

T_0: room temperature

T_C: maximum column temperature minus ionization temperature

T_i: ionization temperature

δ: cathode boundary layer thickness

ΔR: critical radius minus column radius

ΔR_g: length of temperature gradient in gas

μ: viscosity of the plasma at the maximum temperature in the arc

μ_0: permitivity of free space

ρ: density of the plasma at the maximum temperature in the arc

σ_e: electric conductivity of the plasma at the maximum temperature in the arc

σ_T: temperature coefficient of the electric conductivity of the plasma

REFERENCES

1. Mendez, P.F. "*Order of Magnitude Scaling of Complex Engineering Problems, and its Application to High Productivity Arc Welding*." Doctor of Philosophy dissertation. Cambridge, MA. Massachusetts Institute of Technology. 1999.
2. Mendez, P.F. and Eagar, T.W. "Order of Magnitude Scaling." *http://lyre.mit.edu/~pat/Publications/Papers/2002omsI.pdf*. In preparation. 2001.
3. Erdélyi, A. "*Asymptotic expansions*." Dover Publications. New York. 1956.
4. Segel, L.A. "Simplification and Scaling." *SIAM Review*. 14 (4), pp. 547-571. 1972.
5. Bender, C.M. and Orszag, S.A. "*Advanced Mathematical Methods for Scientists and Engineers*." McGraw-Hill. New York. 1978.

6. Barenblatt, G.I. "*Scaling, Self-Similarity, and Intermediate Asymptotics*." Cambridge University Press. New York. 1996.
7. Ruark, A.E. "Inspectional Analysis: A Method which Supplements Dimensional Analysis." *Journal of the Mitchell Society*. 51, pp. 127-133. 1935.
8. Kline, S.J. "*Similitude and Approximation Theory*." Springer-Verlag. New York. 1986.
9. Chen, M.M. "Scales, Similitude, and Asymptotic Considerations in Convective Heat Transfer," in *Annual Review of Heat Transfer*, Vol. 3. Hemisphere Pub. Corp., New York. pp. 233-291. 1990.
10. Astarita, G. "Dimensional Analysis, Scaling, and Orders of Magnitude." *Chemical Engineering Science*. 52 (24), pp. 4681-4698. 1997.
11. Bobrow, D. "*Qualitative Reasoning about Physical Systems*." MIT Press. Cambridge, MA. 1985.
12. Kuipers, B. "Qualitative Simulation." *Artificial Intelligence*. 29, pp. 289-388. 1986.
13. Dague, P. and Raiman, O. "Troubleshooting: When Modeling is the Trouble." *AAAI-87, Sixth National Conference on Artificial Intelligence*, Seattle, WA. American Association for Artificial Intelligence. pp. 600-605. 1987.
14. Kokar, M.M. "Critical Hypersurfaces and the Quantity Space." *AAAI-87, Sixth National Conference on Artificial Intelligence*, 1987.
15. Kokar, M.M. "Generating Qualitative representations of Continuous Physical Processes." *Metodologies for Intelligent Systems*, 1987.
16. Mavrovouniotis, M.L. and Stephanopoulos, G. "Formal Order-of-Magnitude Reasoning in Process Engineering." *Computers & Chemical Engineering*. 12 (9-10), pp. 867-880. 1988.
17. Weld, D.S. "Exaggeration." *Artificial Intelligence*. 43 (3), pp. 311-368. 1990.
18. Weld, D.S. and de Kleer, J. "*Qualitative Reasoning about Physical Systems*." Morgan Kaufmann Publishers, Inc. San Mateo, CA. 1990.
19. Raiman, O. "Order of Magnitude Reasoning." *Artificial Intelligence*. 51 (1-3), pp. 11-38. 1991.
20. Parsons, S. "Using Interval Algebras to Model Order of Magnitude Reasoning." *Artificial Intelligence in Engineering*. 8 (2), pp. 87-98. 1993.

21. Kalagnanam, J.R. and Diwekar, U.M. "An Optimization Approach to Order of Magnitude Reasoning." *Ai Edam-Artificial Intelligence For Engineering Design Analysis and Manufacturing*. 8 (3), pp. 207-217. 1994.
22. Williams, B.C. and Raiman, O. "Decompositional Modeling through Caricatural Reasoning." *Twelft National Conference on Artificial intelligence*, Seattle, WA. pp. 1199-1204. 1994.
23. Yip, K.M.K. "Model Simplification by Asymptotic Order of Magnitude Reasoning." *Artificial Intelligence*. 80 (2), pp. 309-348. 1996.
24. Rudolph, S. "On the Context of Dimensional Analysis in Artificial Intelligence." *International Workshop on Similarity Methods*, 1998.
25. Davis, E. "Order of magnitude comparisons of distance." *Journal of Artificial Intelligence Research*. 10, pp. 1-38. 1999.
26. Mendez, P.F., Ramirez, M.A., Trapaga, G., and Eagar, T.W. "Order of Magnitude Scaling of the Cathode Region in an Axisymmetric Transferred Electric Arc." *Metallurgical Transactions B*. 32B, pp. 547-554. 2001.
27. Squire, H.B. "The Round Laminar Jet." *Quarterly Journal of Mechanics and Applied Mathematics*. IV (3), pp. 321-329. 1951.
28. Maecker, H. "Plasmastromungen in Lichtbogen infolge eigenmagnetischer Kompression." *Zeitschrift fur Physik*. 141, pp. 198-216. 1955.
29. Yas'ko, O.I. "Correlation of the Characteristics of Electric Arcs." *British Journal of Applied Physics (Journal of Physics D: Applied Physics)*. 2 (2), pp. 733-751. 1969.
30. Shercliff, J.A. "Fluid Motions due to an Electric Current Source." *Journal of Fluid Mechanics*. 40 (2), pp. 241-250. 1970.
31. Strachan, D.C. and Barrault, M.R. "Axial Velocity Variations in High-Current Free-Burning Arcs." *Journal of Physics D: Applied Physics*. 9, pp. 435-446. 1976.
32. Burleigh, T.D. "*Measurement of the Arc Force in GTA Welding*." Master of Science dissertation. Cambridge, MA. Massachusetts Institute of Technology. 1980.
33. Allum, C.J. "Gas Flow in the Column of a TIG Welding Arc." *J. Phys. D: Appl. Phys.* 14, pp. 1041-1059. 1981.

34. McKelliget, J.W. and Szekely, J. "A Mathematical Model of the Cathode Region of a High Intensity Carbon Arc." *Journal of Physics D: Applied Physics*. 16, pp. 1007-1022. 1983.
35. Bowman, B. "Properties of Arcs in DC Furnaces." *52nd Electric Furnace Conference*, Nashville, TN. pp. 111-120. 13-16 Nov., 1994.
36. Hsu, K.C., Etemadi, K., and Pfender, E. "Study of the Free-Burning High-Intensity Argon Arc." *Journal of Applied Physics*. 54 (3), pp. 1293-1301. 1983.
37. McKelliget, J. and Szekely, J. "The Modelling of Fluid Flow and Heat Transfer in Arc Furnaces." *5th Arc Furnace Meeting*, Budapest, Hungary. 24-27 September, 1985, 1985.
38. Goodarzi, M., Choo, R., and Toguri, J.M. "The Effect of the Cathode Tip Angle on the GTAW Arc and Weld Pool: I. Mathematical Model of the Arc." *Journal of Physics D: Applied Physics*. , pp. 2744-2756. 1997.
39. Kim, W.-H., Fan, H.G., and Na, S.-J. "A Mathematical Model of Gas Tungsten Arc Welding Considering the Cathode and the Free Surface of the Weld Pool." *Metallurgical Transactions B*. 28B, pp. 679-686. 1997.
40. Lowke, J.J., Morrow, R., and Haidar, J. "A Simplified Unified Theory of Arcs and their Electrodes." *Journal of Physics D: Applied Physics*. 30, pp. 2033-2042. 1997.
41. McKelliget, J. and Szekely, J. "Heat Transfer and Fluid Flow in the Welding Arc." *Metallurgical Transactions A*. 17A, pp. 1139-1147. 1986.
42. Jordan, G.R., Bowman, B., and Wakelam, D. "Electrical and Photographic Measurements of High Power Arcs." *Journal of Physics D: Applied Physics*. 3, pp. 1089-1099. 1970.
43. Moffat, C. "Heat Transfer in Magnetohydrodynamic Fluids," in *Developments in Heat Transfer*, MIT Press, Cambridge, MA. pp. 107-133. 1964.
44. Morrow, R. and Lowke, J.J. "A One-Dimensional Theory for the Electrode Sheaths of Electric Arcs." *Journal of Physics D: Applied Physics*. 26, pp. 634-642. 1993.
45. Haddad, G.N. and Farmer, A.J.D. "Temperature Determinations in a Free-Burning Arc .1. Experimental-Techniques and Results in Argon." *Journal of Physics D-Applied Physics*. 17 (6), pp. 1189-1196. 1984.

46. Choo, R.T.C., Szekely, J., and Westhoff, R.C. "On the Calculation of the Free Surface Temperature of Gas-Tungsten-Arc Weld Pools from First Principles: Part I. Modeling the Welding Arc." *Metallurgical Transactions B*. 23B, pp. 357-369. 1992.
47. Zhu, P. and Lowke, J.J. "Theoretical Study of the Melting of the Cathode Tip of a Free Burning Arc in Argon for Various Conical Angles." 26, pp. 1073-1076. 1993.
48. Lee, S.-Y. and Na, S.-J. "A Numerical Analysis of a Stationary Gas Tungsten Arc Considering Various Electrode Angles." *Welding Journal*. , pp. 269s-279s. 1996.
49. Fan, H.G., Na, S.J., and Shi, Y.W. "Numerical simulation of current density in gas tungsten are welding including the influence of the cathode." *Proceedings of the Institution of Mechanical Engineers Part B- Journal of Engineering Manufacture*. 211 (4), pp. 321-327. 1997.
50. Ramirez, M.A. "*Mathematical Modeling of D. C. Electric Arc Furnace Operations*." Doctor of Philosophy dissertation. Cambridge, MA. Massachusetts Institute of Technology. 2000.

Table I
Boundary conditions for the scaling of the electromagnetic field

	A	B	C	D
B	0	$\frac{1}{2}\mu_0 J_C R_C$	$\frac{1}{2}\mu_0 J_C R_C^2 / R_a$	0

Table II
Boundary conditions for scaling of the fluid flow in the transition region

	E	**F**	**G**	**H**
V_R	0	$\approx -V_{RS}$	≈ 0	0
V_Z	≈ 0	≈ 0	≈ 0	$\approx V_{ZS}$

Table III
Boundary conditions for scaling of the temperature in the column

	H	**L**	**M**	**N**	**O**	**P**
T	$\approx T_i + T_C$	$\approx T_i$	$\approx T_i$	$\approx T_i + T_C$	$\approx T_0$	$\approx T_0$

Table IV
Boundary conditions for numerical representation of the arc. The domain segments make reference to Fig. 1

	AB	BI	IJ	JK	DK	AD	BJ
V_Z	0	0	$\partial V_Z/\partial Z = 0$	$\partial V_Z/\partial R = 0$	0	$\partial V_Z/\partial R = 0$	-
V_R	0	0	0	$\partial V_Z/\partial Z = 0$	0	0	-
T	4000	$\partial T/\partial Z = 0$	1000	1000	2500	$\partial T/\partial R = 0$	-
B	$\mu_o Ir/2\pi R_c^2$	-	-	$\mu_o I/2\pi r$	$\partial B/\partial Z = 0$	B=0	$\mu_o I/2\pi r$

Table V
Characteristic values obtained through numerical analysis

gas	electrode	I [A]	h [m]	T_{max} [K]	ρ [kg/m^2]	μ [kg/m s]	R_C [m]	Z_S [m]	V_{RS} [m/s]	V_{ZS} [m/s]	P_S [Pa]
Argon	W	200	0.01	21600	1.12E-02	5.41E-05	9.897E-04	1.22E-03	76	256	574
Argon	W	200	0.02	21500	1.12E-02	5.41E-05	9.897E-04	1.47E-03	80	266	597
Argon	W	300	0.0063	23200	9.97E-03	4.59E-05	1.212E-03	1.30E-03	101	353	1084
Argon	W	300	0.01	23200	9.97E-03	4.59E-05	1.212E-03	1.49E-03	104	363	1062
Argon	W	300	0.02	23100	9.97E-03	4.59E-05	1.212E-03	1.75E-03	105	372	989
air	C	520	0.07	17200	5.70E-03	3.26E-05	1.940E-03	4.76E-03	170	574	1492
air	C	1150	0.07	19500	4.71E-03	1.87E-05	2.884E-03	5.43E-03	247	983	3653
air	C	2160	0.07	21300	4.23E-03	1.64E-05	3.953E-03	7.09E-03	318	1498	7524

Table VI
Thermal properties of plasma [50]

parameter	units	Ar	Air
k_T	W/mK^2	2×10^{-4}	6.875×10^{-4}
σ_T	A^2/WmK	0.769	0.777
S_{RT}	W/m^3K	0.93×10^{6}	0.25×10^{6}
$(5/2\ k_b/e)$	W/AK	2.15×10^{-4}	2.15×10^{-4}
k_g	W/mK	0.913	4
S_{Rg}	W/m^3	2×10^{8}	2×10^{8}
T_i,	K	11000	7000

Table VII
Coefficients and correlation factor for the estimations

magnitude	coefficient $\left(\frac{\text{measurement or calculation}}{\text{estimation}}\right)$	R^2
$\hat{Z}_S$	3.5863	0.9071
$\hat{V}_{RS}$	0.2266	0.9753
$\hat{V}_{ZS}$	0.9427	0.9821
$\hat{P}_S$	0.3706	0.9738
$\hat{R}_i$	0.6049	0.9191
$\hat{T}_C$	1.0204	0.3667
$\Delta\hat{R}_g$	1.1386	0.1815

Table VIII

Summary of magnitudes, associated functions, characteristic values, and estimations used in the formulation of the problem

Magnitude	Symbol	Normalized magnitude	Characteristic value	Estimated characteristic value
Radial coordinate	R	r	R_C	
		r'	R_i	$\hat{R}_i$
		r''	ΔR_g	$\Delta\hat{R}_g$
Axial coordinate	Z	z	Z_S	$\hat{Z}_S$
Radial velocity	$V_R(R, Z)$	$v_r(r, z)$	V_{RS}	$\hat{V}_{RS}$
Axial velocity	$V_Z(R, Z)$	$v_z(r, z)$		
		$v_{z0}(z)$	V_{ZS}	$\hat{V}_{ZS}$
Pressure	$P(R, Z)$	$p(r, z)$	P_S	$\hat{P}_S$
Temperature	T	θ'	T_C	$\hat{T}_C$
		θ''	T_i-T_0	
Radial current density	$J_R(R, Z)$	$j_r(r, z)$	J_{RS}	$\hat{J}_{RS}$
Axial current density	$J_Z(R, Z)$	$j_z(r, z)$	J_C	
Magnetic flux density	$B(R, Z)$	$b(r, z)$	B_S	

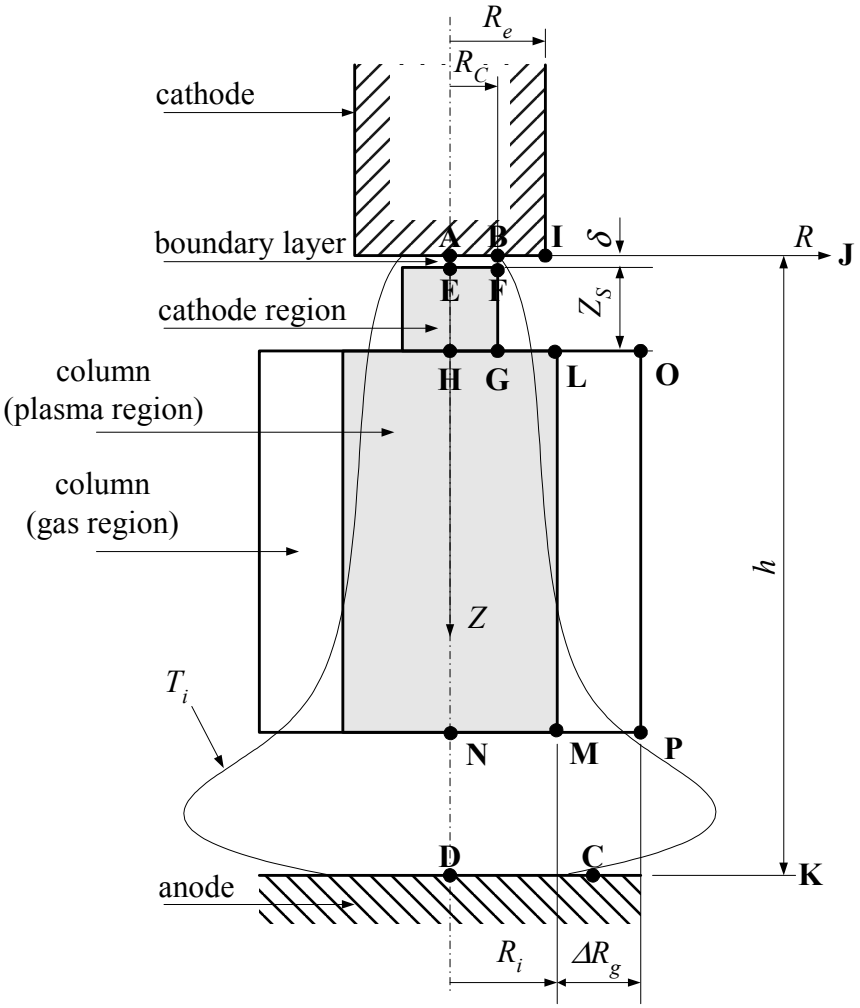

Fig. 1 - Long GTA welding arc , and its transition region. In a long arc the arc length (h) is significantly longer than the characteristic distance Z_S

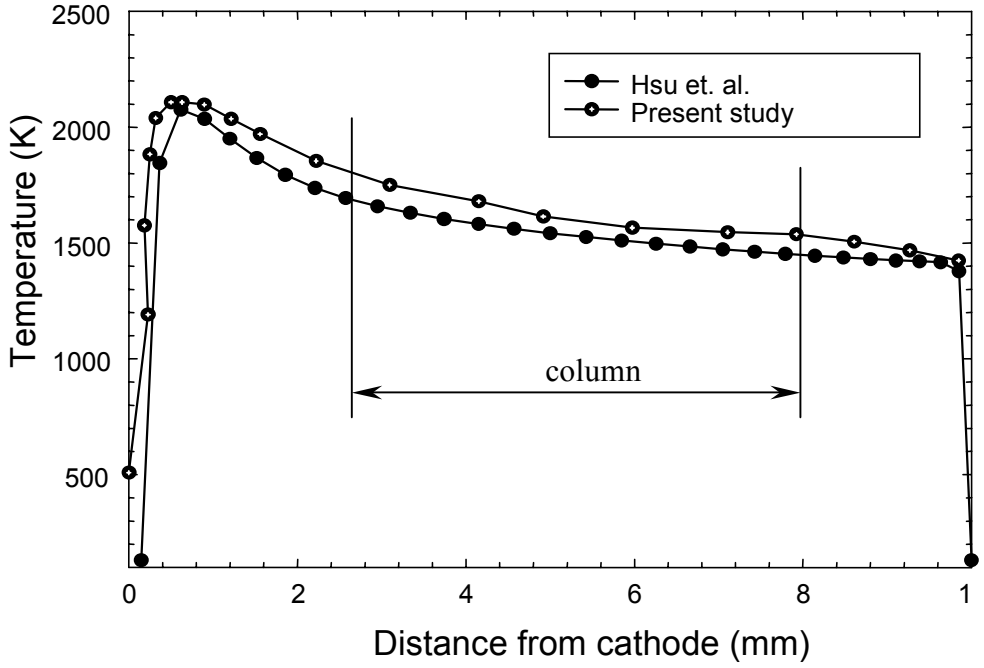

Fig. 2: Temperature distribution along the axis of symmetry

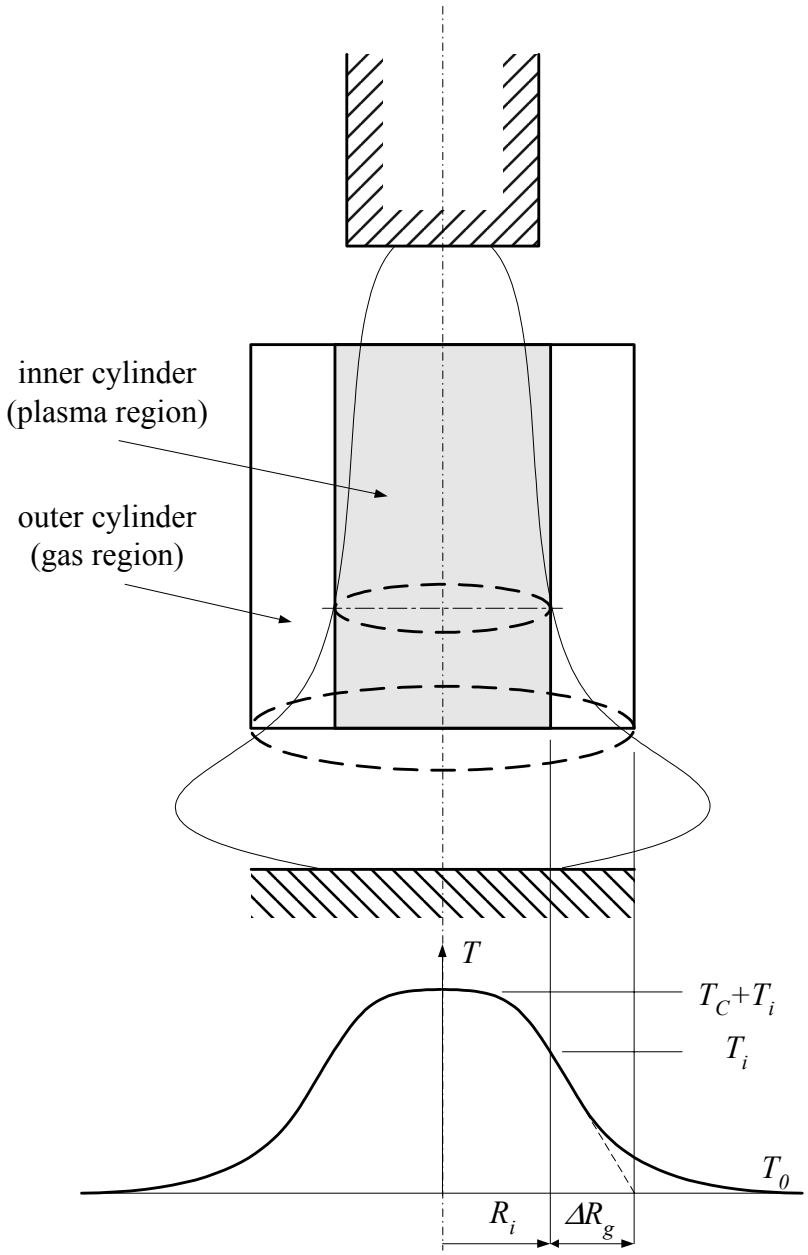

Fig. 3: Inner and outer cylinders containing the plasma and gas regions of the arc column

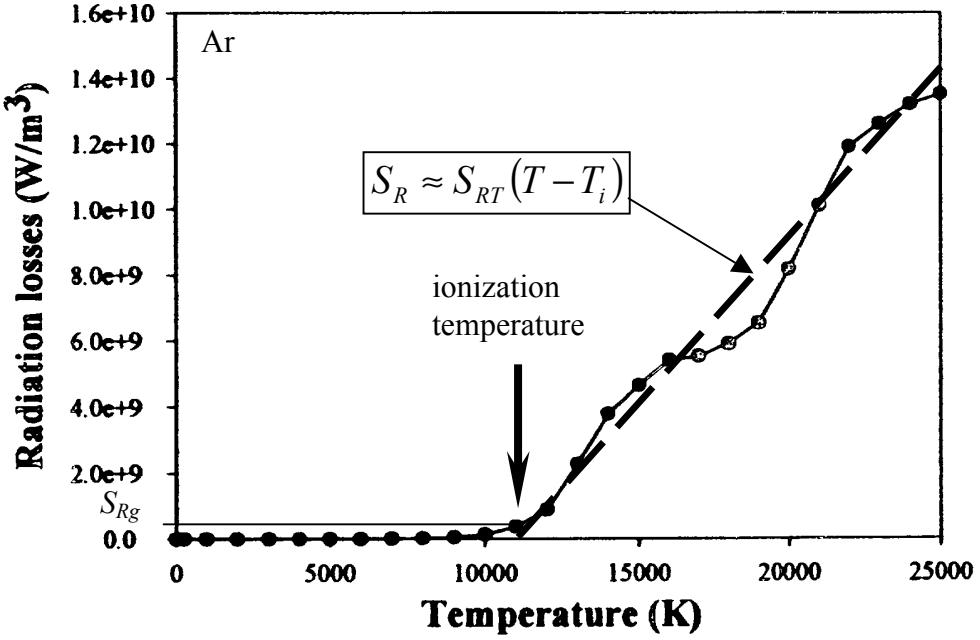

Fig. 4: Definition of ionization temperature. Argon plasma properties from [50]

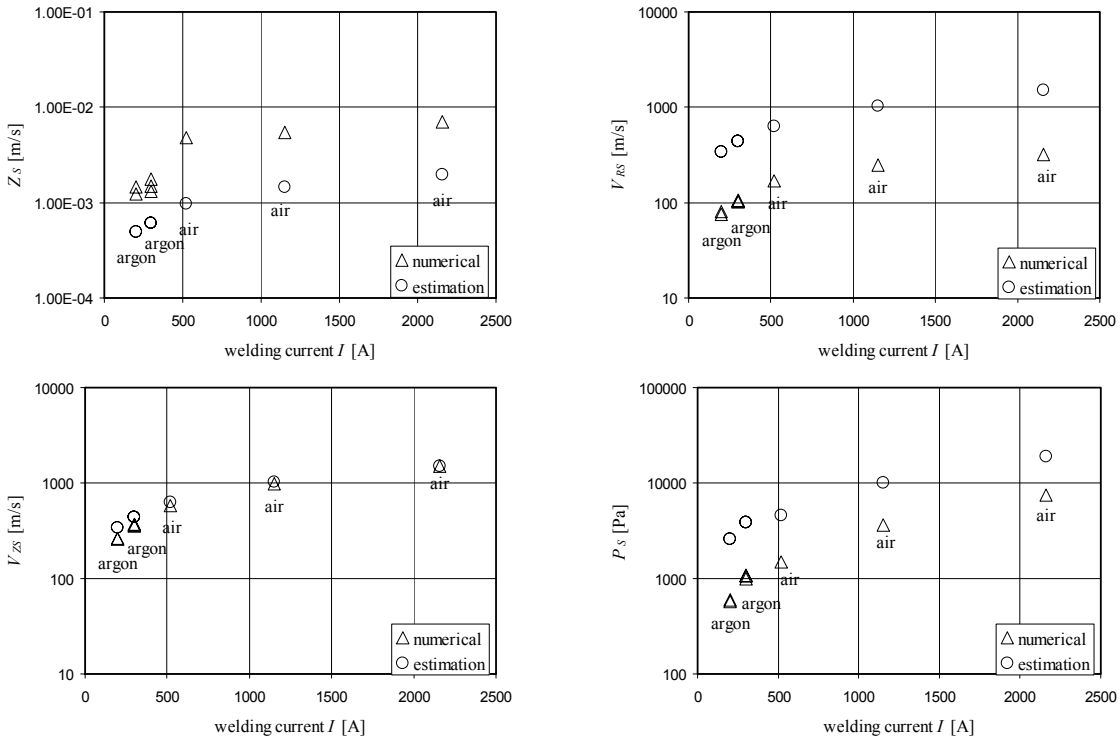

Fig. 5 - Estimations and numerical calculations of V_{RS}, V_{ZS}, P_S, and Z_S. In all cases the estimations predict the correct order of magnitude and functional dependence.

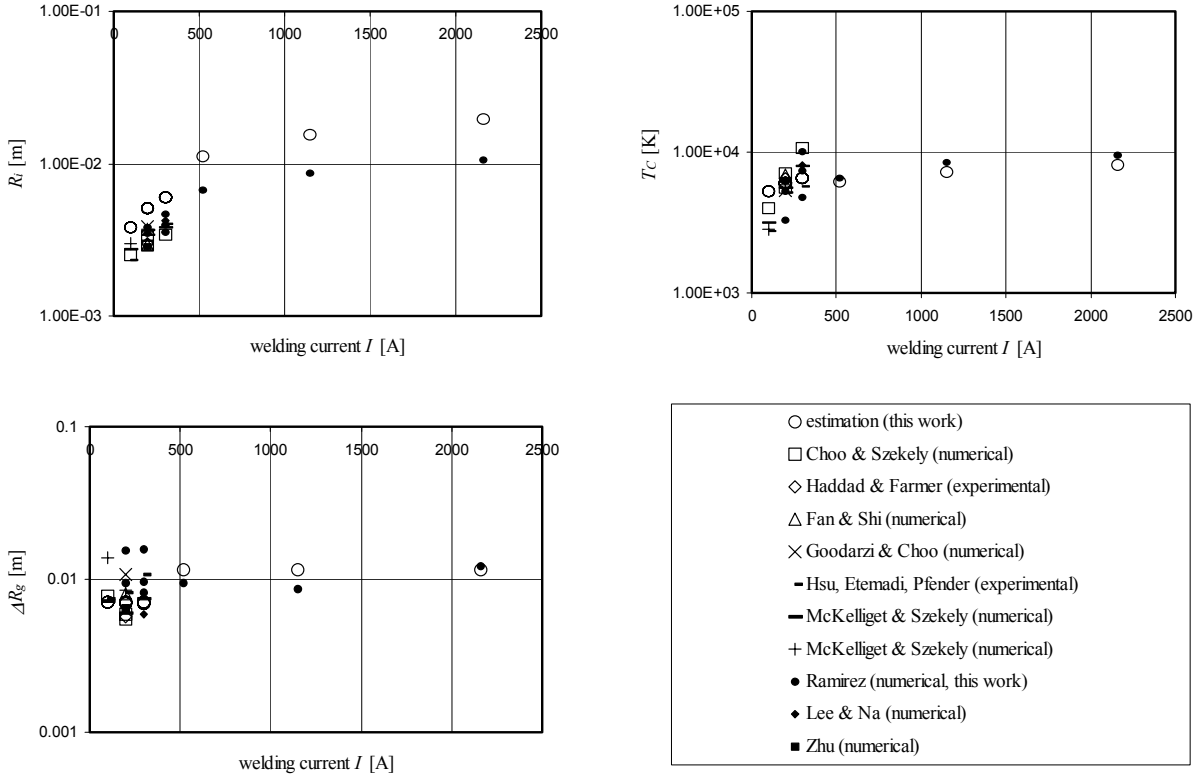

Fig. 6 Estimations and numerical calculations of R_i, T_C, and ΔR_g. In all cases the estimations predict the correct order of magnitude.